Inorganic Chemistry

Article

Mixed Cations and Structural Complexity in $(Eu_{1-x}Ca_x)_4In_3Ge_4$ and $(Eu_{1-x}Ca_x)_3In_2Ge_3$—The First Two Members of the Homologous Series $A_{2[n+m]}In_{2n+m}Ge_{2[n+m]}$ ($n, m = 1, 2, ...\infty$; A = Ca, Sr, Ba, Eu, or Yb)

Tae-Soo You, Paul H. Tobash, and Svilen Bobev*

Department of Chemistry and Biochemistry, University of Delaware, Newark, Delaware 19716

Reported are the synthesis and the structural characterization of two members of a new homologous series of polar intermetallic compounds, which exist only with mixed alkaline-earth and rare-earth metal cations. Crystals of $(Eu_{1-x}Ca_x)_4In_3Ge_4$ ($0.35(1) \leq x \leq 0.70(1)$) and $(Eu_{1-x}Ca_x)_3In_2Ge_3$ ($0.78(1) \leq x \leq 0.90(1)$) have been grown using a molten In metal flux and structurally characterized by single-crystal X-ray diffraction. $(Eu_{1-x}Ca_x)_4In_3Ge_4$ adopts the monoclinic Mg_5Si_6-type structure (space group $C2/m$, $Z = 2$, Pearson symbol $mS22$) with lattice parameters $a = 16.874(1)-17.024(2)$ Å, $b = 4.496(3)-4.556(1)$ Å, $c = 7.473(4)-7.540(1)$ Å, and $\beta = 107.306(10)-105.631(3)°$. $(Eu_{1-x}Ca_x)_3In_2Ge_3$ crystallizes with a novel orthorhombic structure (space group $Pnma$, $Z = 4$, Pearson symbol $oP32$) with lattice parameters in the ranges $a = 7.382(2)-7.4010(9)$ Å, $b = 4.452(1)-4.4640(6)$ Å, and $c = 23.684(6)-23.734(3)$ Å, depending on the Eu/Ca ratio. The polyanionic substructures in both cases are related and are based on $InGe_4$ edge-shared tetrahedra, Ge_2 dimers, and bridging In atoms in a nearly square-planar environment. The $(Eu_{1-x}Ca_x)_4In_3Ge_4$ structure can be viewed as a 1:1 intergrowth of Mo_2FeB_2-like and TiNiSi-like fragments, whereas $(Eu_{1-x}Ca_x)_3In_2Ge_3$ can be rationalized as a 2:1 intergrowth of the same structural motifs. Both phases exhibit fairly wide homogeneity ranges and exist only with mixed cations. The experimental results have been complemented by linear muffin-tin orbital tight-binding band structure calculations, as well as an analysis of the observed cationic site preferences.

Introduction

Intermetallic compounds offer numerous opportunities to explore composition−structure−chemical bonding relationships.[1] Among all classes of intermetallic compounds, polar intermetallics, which can be regarded as an intermediate between the Zintl phases[2] and the Hume−Rothery (electronic) or Laves (geometric) phases, are particularly amenable to such studies. Typical polar intermetallics consist of electropositive metals, such as the alkali, alkaline-earth, and rare-earth elements, and electronegative metals from the late transition metals and early post-transition metal elements near the Zintl border, that is, Al, Si, and Ge.[3] As a consequence of this relatively large electronegativity differential, the chemical bonding in such compounds exhibits three characteristic features: (i) Bonding within the network of electronegative (poly)anions is optimized at the Fermi level, resulting in a sharp distinction between filled bonding states and empty antibonding states. (ii) There is no apparent energy gap separating the valence and the conduction bands; however, the density of states curves often show a minimum value at the Fermi level (usually referred to as a pseudogap). (iii) The electropositive metals may not contribute all of their valence electrons to the network of electronegative polyanions.[4]

In the past 5 years, our group has studied a number of alkaline-earth and rare-earth metal compounds, which belong to the class of polar intermetallics.[5−12] More specifically, when

*To whom correspondence should be addressed. Phone: (302) 831-8720. Fax: (302) 831-6335. E-mail: bobev@udel.edu.

(1) Westbrook, J. H.; Fleischer, R. L. *Intermetallic Compounds: Principle and Practice*; Wiley: New York, 1995.

(2) (a) Schäfer, H. *Annu. Rev. Mater. Sci.* **1985**, *5*, 1. (b) Nesper, R. *Prog. Solid State Chem.* **1990**, *20*, 1. (c) Kauzlarich, S. M. *Chemistry, Structure and Bonding in Zintl Phases and Ions*; VCH: New York, 1996, and the references therein.

(3) Miller, G. J.; Lee, C.-S.; Choe, W. In *Inorganic Chemistry Highlights*; Meyer, G., Naumann, D., Wesemann, L., Eds.; Wiley-VCH: Berlin, 2002.

(4) Klem, M. T.; Vaughy, J. T.; Harp, J. G.; Corbett, J. D. *Inorg. Chem.* **2001**, *40*, 7020.

(5) Tobash, P. H.; Lins, D.; Bobev, S.; Lima, A.; Hundley, M. F.; Thompson, J. D.; Sarrao, J. L. *Chem. Mater.* **2005**, *17*, 5567.

(6) Xia, S.-Q.; Bobev, S. *J. Solid State Chem.* **2006**, *179*, 3371.

(7) Bobev, S.; Merz, J.; Lima, A.; Fritsch, V.; Thompson, J. D.; Sarrao, J. L.; Gillessen, M.; Dronskowski, R. *Inorg. Chem.* **2006**, *45*, 4047.

(8) Tobash, P. H.; Bobev, S. *J. Am. Chem. Soc.* **2006**, *128*, 3252.

(9) Tobash, P. H.; Meyers, J. J.; DiFilippo, G.; Bobev, S.; Ronning, F; Thompson, J. D.; Sarrao, J. L. *Chem. Mater.* **2008**, *20*, 2151.

(10) Tobash, P. H.; Bobev, S.; Thompson, J. D.; Sarrao, J. L. *Inorg. Chem.* **2009**, *48*, 6641.

(11) Bobev, S.; Xia, S.-Q.; Bauer, E. D.; Ronning, F.; Thompson, J. D.; Sarrao, J. L. *J. Solid State Chem.* **2009**, *182*, 1473.

(12) Xia, S.-Q.; Myers, C.; Bobev, S. *Eur. J. Inorg. Chem.* **2008**, 4262.

the metal-flux technique[13] was used and when the relative "inertness" of the In flux was relied upon,[14] several new binary germanides were synthesized for the first time.[15,16] During the exploratory work, in addition to the binary phases, the ternary compounds RE_2InGe_2 (RE = Sm, Gd−Ho, Yb)[5] were also identified. Systematic investigation of the RE−In−Ge systems[5,17] showed that the Mo_2FeB_2-type structure,[18] in which the RE_2InGe_2 phases crystallize, can be realized only with the early-to-mid late rare-earth metals. Similar structural trends have also been reported for the isostructural RE_2MgGe_2[19] and RE_2MgNi_2[20] phases. These findings suggest that optimization of the lattice energy likely cannot be achieved when the very late and rather small 4f elements Er, Tm, and Lu are used. The same reasoning, namely, the much larger size of Eu^{2+} compared to that of Yb^{2+}, the other nominally divalent rare-earth metal ion,[21] can explain the observation that Yb_2InGe_2 exists,[5] but the synthesis of Eu_2InGe_2 was unsuccessful. However, the same arguments seem inadequate when comparing Ca_2InGe_2 and Yb_2InGe_2—because of the nearly identical radii of Ca^{2+} and Yb^{2+},[21] the crystal packing in both cases is expected to be similar, yet, only the latter is known. All of the above, together with the results from electronic structure calculations,[19a,22] indicate that the chemical bonding in this simple structure is rather complicated and involves substantial cation contributions. These facts piqued our attention, and having recently studied other polar intermetallic phases with intricate cation−anion interactions,[23−26] we set out to investigate the systems Eu−Ca−Ge and Eu−Yb−Ge employing molten In as a flux. Such studies with mixtures of chemically similar but spatially different cations were inspired by the success in employing mixed alkali metals and alkaline-earth metals in the synthesis of novel clusters,[27] chains,[28] or frameworks[27,29] of the early post-transition elements. In this article, we have detailed the initial results of this work, discussing the synthetic efforts and the single-crystal structures of the new phases

$(Eu_{1−x}Ca_x)_4In_3Ge_4$ $(0.35(1) \leq x \leq 0.70(1))$ and $(Eu_{1−x}Ca_x)_3In_2Ge_3$ $(0.78(1) \leq x \leq 0.90(1))$. Presented as well are their homogeneity ranges, their electronic structures, and the cation site preferences in each case, rationalized using the *coloring concept.*[30]

Experimental Section

Synthesis. All manipulations were performed inside an argon-filled glovebox or under a vacuum. The starting materials—pure elements from Alfa or Aldrich (>99.9%)—were used as received. The flux reactions were carried out in 2 cm^3 alumina crucibles, using appropriate ratios of the alkaline-earth and rare-earth metals and germanium, and typically, a 10-fold excess of In. Additional reactions, aimed at synthesizing the title compounds without the use of metal flux, and establishing the phase widths, were carried out by loading all elements in stoichiometric ratios in Nb ampules. In both types of experiments, the reaction containers were subsequently enclosed in fused silica ampules and flame-sealed under a vacuum, before being heated to the desired temperatures. Since numerous reactions were set up, and a number of heat treatments explored, only a brief and general description of the synthesis of $(Eu_{1−x}Ca_x)_4In_3Ge_4$ and $(Eu_{1−x}Ca_x)_3In_2Ge_3$ is given below. Detailed experimental procedures and temperature profiles are provided in the Supporting Information.

The new $(Eu_{1−x}Ca_x)_4In_3Ge_4$ phase ("4−3−4" phase) was serendipitously discovered as the main product of an In flux reaction of Eu, Ca, and Ge in an equimolar ratio. In this first attempt, the mixture of the elements was heated in a muffle furnace to 960 °C and held at this temperature for 20 h, then slowly cooled to 500 °C. At this point, the molten In was removed, and many needle-shaped crystals with a silver luster were isolated. After the structure and the composition were confirmed by X-ray crystallography, the synthesis of the new compound was reproduced from an on-stoichiometry reaction in a sealed Nb ampule. Experiments aimed at pure ternary $Eu_4In_3Ge_4$ or $Ca_4In_3Ge_4$ phases were not successful at these reaction conditions—they afforded the known binary phase $EuGe_2$[31] and the hexagonal polytype of $CaGe_2$[32] instead. Other reactions with varied Eu and Ca ratios also produced the targeted phase, although $EuGe_2$ and $CaGe_2$ (or rather the solid solutions $Eu_{1−x}Ca_xGe_2$) were always formed as side products. In particular, the latter were the main products of all reactions set up with more than 90 atom % Eu or 95 atom % Ca ($Eu_{1−x}Ca_xInGe$, isostructural with $EuInGe$[33] was also identified as a byproduct of the Eu-rich reactions). To the contrary, the Ca-rich reactions yielded another new phase, later identified as $(Eu_{1−x}Ca_x)_3In_2Ge_3$ ("3−2−3" phase).

The elaborate synthetic efforts helped establish the homogeneity ranges for the "4−3−4" and "3−2−3" phases. Although not exhaustive, our experiments suggest $(Eu_{1−x}Ca_x)_4In_3Ge_4$ to exist at Eu/Ca ratios varying from about 2:1 to 1:2, respectively, while $(Eu_{1−x}Ca_x)_3In_2Ge_3$ exists only for Ca-rich compositions ranging from Eu/Ca ≈ 1:9 to Eu/Ca ≈ 1:3. Similarly complicated phase relationships were established for the Sr−Ca−In−Ge and Eu−Yb−In−Ge systems, which are still under investigation. Preliminary results indicate that compounds isostructural to either the "4−3−4" or the "3−2−3" phase do *not* exist in these systems, which is unexpected given how close the ionic radii are: $r = 1.16$ Å for Eu^{2+} versus $r = 1.17$ Å for Sr^{2+} on one side and $r = 1.00$ Å for Yb^{2+} versus $r = 1.02$ Å for Ca^{2+} on the other.[21] More experimental results for

(13) (a) Canfield, P. C.; Fisk, Z. *Philos. Mag. B* **1992**, *65*, 1117. (b) Kanatzidis, M. G.; Pöttgen, R.; Jeitschko, W. *Angew. Chem., Int. Ed.* **2005**, *44*, 6996.

(14) Reflected in the infrequency of side reactions with the alkaline-earth and rare-earth metals, or the inclusion of indium in the products' structures.

(15) (a) Tobash, P. H.; Lins, D.; Bobev, S.; Hur, N.; Thompson, J. D.; Sarrao, J. L. *Inorg. Chem.* **2006**, *45*, 7286. (b) Tobash, P. H.; Bobev, S.; Ronning, F.; Thompson, J. D.; Sarrao, J. L. *J. Alloys Compd.* **2009**, *488*, 533.

(16) Tobash, P. H.; DiFilippo, G.; Bobev, S.; Hur, N.; Thompson, J. D.; Sarrao, J. L. *Inorg. Chem.* **2007**, *46*, 8690.

(17) Zaremba, V. I.; Kaczorowski, D.; Nychyporuk, G. P.; Rodewald, U. C.; Poettgen, R. *Solid State Sci.* **2004**, *6*, 1301.

(18) Villars, P.; Calvert, L. D. *Pearson's Handbook of Crystallographic Data for Intermetallic Phases*, 2nd ed.; American Society for Metals: Materials Park, OH, 1991.

(19) (a) Choe, W.; Miller, G. J.; Levin, E. M. *J. Alloys Compd.* **2001**, *329*, 121. (b) Kraft, R.; Pöttgen, R. *Montash. Chem.* **2004**, *135*, 1327.

(20) Hoffmann, R.-D.; Fugmann, A.; Rodewald, U. C.; Pöttgen, R. *Z. Anorg. Allg. Chem.* **2000**, *626*, 1733.

(21) Shannon, R. D. *Acta Crystallogr., Sect. A* **1976**, *32*, 751.

(22) Whangbo, M.-H.; Lee, C.; Köhler, J. *Angew. Chem., Int. Ed.* **2006**, *45*, 7465.

(23) Xia, S.-Q.; Bobev, S. *J. Am. Chem. Soc.* **2007**, *129*, 4049.

(24) Xia, S.-Q.; Bobev, S. *J. Am. Chem. Soc.* **2007**, *129*, 10019.

(25) Xia, S.-Q.; Bobev, S. *Inorg. Chem.* **2008**, *47*, 1919.

(26) Tobash, P. H.; Bobev, S.; Ronning, F.; Thompson, J. D.; Sarrao, J. L. *J. Alloys Compd.* **2009**, *488*, 511.

(27) Corbett, J. D. *Angew. Chem., Int. Ed.* **2000**, *39*, 670 and the references therein.

(28) Xu, Z.; Guloy, A. M. *J. Am. Chem. Soc.* **1997**, *119*, 10541.

(29) Bobev, S.; Sevov, S. C. *J. Am. Chem. Soc.* **1999**, *121*, 3795.

(30) Miller, G. J. *Eur. J. Inorg. Chem.* **1998**, *5*, 523.

(31) Bobev, S.; Bauer, E. D.; Thompson, J. D.; Sarrao, J. L.; Miller, G. J.; Eck, B.; Dronskowski, R. *J. Solid State Chem.* **2004**, *177*, 3545.

(32) Tobash, P. H.; Bobev, S. *J. Solid State Chem.* **2007**, *180*, 1575.

(33) Mao, J.-G.; Goodey, J.; Guloy, A. M. *Inorg. Chem.* **2002**, *41*, 931.

Table 1. Selected Crystal Data and Structure Refinement Parameters for the Most Eu- and Ca-Rich Members of the $(Eu_{1-x}Ca_x)_4In_3Ge_4$ ($0.35 \leq x \leq 0.70$) and $(Eu_{1-x}Ca_x)_3In_2Ge_3$ ($0.78 \leq x \leq 0.90$) Series

empirical formula	$Eu_{1.23(1)}Ca_{2.77}In_3Ge_4$	$Eu_{2.60(1)}Ca_{1.40}In_3Ge_4$	$Eu_{0.30(1)}Ca_{2.70}In_2Ge_3$	$Eu_{0.66(1)}Ca_{2.34}In_2Ge_3$
fw, g mol^{-1}	932.75	1086.03	601.21	642.29
space group	*C2/m* (no. 12)		*Pnma* (no. 62)	
λ, Å		0.71073		
T, K		200(2)		
a, Å	16.874(1)	17.012(2)	7.382(2)	7.4010(9)
b, Å	4.496(3)	4.556(1)	4.4519(12)	4.4640(6)
c, Å	7.473(4)	7.540(4)	23.684(6)	23.734(3)
β, deg	107.306(10)	107.631(3)		
V, Å^3	541.4(5)	556.97(1)	778.4(4)	784.1(2)
Z	2	2	4	4
ρ_{calcd}, g cm^{-3}	5.719	6.476	5.128	5.434
μ (Mo Kα), cm^{-1}	254.4	316.9	213.1	237.6
GOF on F^2	1.074	1.093	1.007	1.060
R_1 [$I > 2\sigma(I)$]^a	0.0311	0.0334	0.0370	0.0320
wR_2 [$I > 2\sigma(I)$]^a	0.0592	0.0586	0.0665	0.0542
R_1 [all data]^a	0.0474	0.0461	0.0724	0.0479
wR_2 [all data]^a	0.0638	0.0625	0.0738	0.0596

$^a R_1 = \sum ||F_o| - |F_c|| / \sum |F_o|$; $wR_2 = [\sum[w(F_o^2 - F_c^2)^2] / \sum[w(F_o^2)^2]]^{1/2}$, and $w = 1/[\sigma^2 F_o^2 + (A \cdot P)^2 + B \cdot P]$, $P = (F_o^2 + 2F_c^2)/3$; A and B are weight coefficients.

these mixed-cation systems are described in the Supporting Information.

Powder X-Ray Diffraction. X-ray powder diffraction patterns were taken at room temperature on a Rigaku MiniFlex powder diffractometer using Cu Kα radiation. The diffractometer was enclosed and operated inside a nitrogen-filled glovebox to handle air- and moisture-sensitive materials. Typical runs included θ–θ scans with scan steps of 0.05° and a 5 s/step counting time. JADE 6.5 was used for data analysis, which indicated that, in almost all cases, the reaction products were complex mixtures of phases. Given the similar structures of the "4–3–4" and "3–2–3" phases, the presence of more than three elements, and the close stoichiometries, these findings are not surprising.

Powder patterns collected for specimens kept under an inert atmosphere and after 72 h of exposure to air were identical, suggesting that the materials are air-stable over this period of time.

Single-Crystal X-Ray Diffraction. Single-crystal X-ray diffraction data were collected at 200 K on a Bruker SMART CCD-based diffractometer. Many crystals from each batch were selected and checked for quality by rapid scans, before the best ones were chosen for further analysis. Monochromated Mo Kα_1 radiation ($\lambda = 0.71073$ Å) was used, and data collections were handled in batch runs at different ω and ϕ angles, controlled by the *SMART* software.[34] The frame width was 0.3–0.4° in ω and θ with a data acquisition rate of 8–12 s/frame. The angular range in 2θ was from ca. 5° to 61°. Intensities were extracted and corrected for Lorentz and polarization effects using the *SAINT* program.[35] Semiempirical absorption correction based on equivalents was applied using *SADABS*.[36] The structure factors were sorted and merged by the program *XPREP* in the *SHELXTL* software package,[37] which was also employed in the space group determination. The structures were solved by direct methods and refined to convergence by full matrix least-squares methods on F^2. Refined parameters included the scale factor, the atomic positions with anisotropic displacement parameters, and occupancy factors for the Eu/Ca positions.

(34) *SMART NT*, version 5.63; Bruker Analytical X-ray Systems, Inc.: Madison, WI, 2003.
(35) *SAINT NT*, version 6.45; Bruker Analytical X-ray Systems, Inc.: Madison, WI, 2003.
(36) *SADABS NT*, version 2.10; Bruker Analytical X-ray Systems, Inc.: Madison, WI, 2001.
(37) (a) *SHELXS-97*; Bruker Analytical Systems, Inc.: Madison, WI, 1990. (b) *SHELXTL*, version 6.12; Bruker Analytical Systems, Inc.: Madison, WI, 2001.

Standardization of the coordinates was done employing *STRUCTURE TIDY*.[38]

Relevant crystallographic data for representative members of the "4–3–4" and "3–2–3" structures are given in Table 1. Final positional and equivalent isotropic displacement parameters and selected interatomic distances are listed in Tables 2 and 3, respectively. Analogous information from structure refinements for intermediate compositions is summarized in the Supporting Information (crystallographic information files, Tables S1–S6). CIFs have also been deposited with Fachinformationszentrum Karlsruhe, 76344 Eggenstein-Leopoldshafen, Germany (fax: (49) 7247–808–666; e-mail: crysdata@fiz.karlsruhe.de) with depository numbers CSD-421159 for $Eu_{2.60(1)}Ca_{1.40}In_3Ge_4$, CSD-421156 for $Eu_{2.40(1)}Ca_{1.60}In_3Ge_4$, CSD-421157 for $Eu_{2.14(1)}Ca_{1.86}In_3Ge_4$, CSD-421158 for $Eu_{2.01(1)}Ca_{1.99}In_3Ge_4$, CSD-421160 for $Eu_{1.73(1)}Ca_{2.27}In_3Ge_4$, CSD-421161 for $Eu_{1.33(1)}Ca_{1.67}In_3Ge_4$, CSD-421162 for $Eu_{1.23(1)}Ca_{2.77}In_3Ge_4$, CSD-421163 for $Eu_{0.66(1)}Ca_{2.34}In_2Ge_3$, CSD-421164 for $Eu_{0.56(1)}Ca_{2.44}In_2Ge_3$, CSD-421165 for $Eu_{0.52(1)}Ca_{2.48}In_2Ge_3$, CSD-421166 for $Eu_{0.30(1)}Ca_{2.70}In_2Ge_3$, CSD-421167 for $Eu_{0.84(1)}Ca_{0.16}Ge_2$, CSD-421168 for $Sr_{0.38(1)}Eu_{0.62}Ge_2$, CSD-421169 for $Eu_{0.84(1)}Ca_{0.16}InGe$, and CSD-421170 for $Ca_{0.50(1)}Yb_{1.50}InGe_2$.

Magnetic Susceptibility Measurements. Field-cooled dc magnetization (M) measurements were performed using a Quantum Design MPMS-2 SQUID magnetometer in the temperature range from 5 to 290 K and in an applied magnetic field (H) of 500 Oe. The raw magnetization data were collected for the holder contribution and converted to molar susceptibility ($\chi_m = M/H$).

Because of the inability to prepare phase-pure material for all compositions, measurements were taken only for two $(Eu_{1-x}Ca_x)_4In_3Ge_4$ batches. In these cases, the phase purity was greater than 95%, as evidenced by the corresponding powder patterns (Supporting Information). In all other instances, more than one phase was present—most commonly $(Eu_{1-x}Ca_x)_4In_3Ge_4$, $(Eu_{1-x}Ca_x)_3In_2Ge_3$, or $Eu_{1-x}Ca_xInGe$. They were not easily distinguishable from one another. This, together with the fact that the flux-grown crystals had similar habits, did not allow for the crystals' mechanical separation under a microscope and hampered further measurements and the identification of possible trends as a function the Eu content.

Elemental Analysis. Large, needle-like single crystals of $(Eu_{1-x}Ca_x)_4In_3Ge_4$ ($x = 0.70(1)$) were picked and mounted onto

(38) Gelato, L. M.; Parthe, E. *J. Appl. Crystallogr.* **1987**, *20*, 139.

Table 2. Atomic Coordinates and Equivalent Isotropic Displacement Parameters (U_{eq}[a]) for the Most Eu- and Ca-Rich Members of the $(Eu_{1-x}Ca_x)_4In_3Ge_4$ ($0.35 \leq x \leq 0.70$) and $(Eu_{1-x}Ca_x)_3In_2Ge_3$ ($0.78 \leq x \leq 0.90$) Series[b]

atom	site	occupation factor	x	y	z	U_{eq} (Å^2)
			$Eu_{1.23(1)}Ca_{2.77}In_3Ge_4$			
M1[c]	4i	0.812(3)/0.188	0.3522(1)	0	0.0788(2)	0.014(1)
M2[c]	4i	0.575(3)/0.425	0.5775(1)	0	0.3648(2)	0.014(1)
In1	4i	1	0.2131(1)	0	0.6234(1)	0.016(1)
In2	2a	1	0	0	0	0.019(1)
Ge1	4i	1	0.0551(1)	0	0.6582(1)	0.013(1)
Ge2	4i	1	0.1908(1)	0	0.2271(1)	0.013(1)
			$Eu_{2.60(1)}Ca_{1.40}In_3Ge_4$			
M1[c]	4i	0.515(3)/0.485	0.3527(1)	0	0.0770(1)	0.014(1)
M2[c]	4i	0.188(4)/0.812	0.5783(1)	0	0.3658(1)	0.014(2)
In1	4i	1	0.2122(1)	0	0.6242(1)	0.013(1)
In2	2a	1	0	0	0	0.020(1)
Ge1	4i	1	0.0543(1)	0	0.6587(2)	0.013(1)
Ge2	4i	1	0.1924(1)	0	0.2303(2)	0.013(1)
			$Eu_{0.30(1)}Ca_{2.70}In_2Ge_3$			
M1[c]	4c	0.918(4)/0.082	0.0121(3)	1/4	0.0723(1)	0.015(1)
M2[c]	4c	0.842(4)/0.158	0.0246(3)	1/4	0.3812(1)	0.015(1)
M3[c]	4c	0.942(4)/0.058	0.1652(3)	1/4	0.2265(1)	0.013(1)
In1	4c	1	0.1502(1)	1/4	0.5271(1)	0.016(1)
In2	4c	1	0.1626(1)	1/4	0.8261(1)	0.018(1)
Ge1	4c	1	0.0372(2)	1/4	0.7101(1)	0.013(1)
Ge2	4c	1	0.2842(2)	1/4	0.6359(1)	0.013(1)
Ge3	4c	1	0.7645(2)	1/4	0.5388(1)	0.014(1)
			$Eu_{0.66(1)}Ca_{2.34}In_2Ge_3$			
M1[c]	4c	0.805(2)/0.195	0.0110(2)	1/4	0.0721(1)	0.016(1)
M2[c]	4c	0.654(3)/0.346	0.0243(1)	1/4	0.3818(1)	0.014(1)
M3[c]	4c	0.878(3)/0.122	0.1642(2)	1/4	0.2265(1)	0.015(1)
In1	4c	1	0.1505(1)	1/4	0.5273(1)	0.015(1)
In2	4c	1	0.1631(1)	1/4	0.8256(1)	0.022(1)
Ge1	4c	1	0.0383(1)	1/4	0.7101(1)	0.014(1)
Ge2	4c	1	0.2846(1)	1/4	0.6363(1)	0.015(1)
Ge3	4c	1	0.7646(1)	1/4	0.5387(1)	0.016(1)

[a] U_{eq} is defined as one-third of the trace of the orthogonalized U_{ij} tensor. [b] The refined atomic coordinates for the intermediate compositions are given as Supporting Information. [c] Refined as a statistical mixture of Ca and Eu.

Table 3. Important Interatomic Distances (Å) in the Most Eu- and Ca-Rich Members of the $(Eu_{1-x}Ca_x)_4In_3Ge_4$ ($0.35 \leq x \leq 0.70$) and $(Eu_{1-x}Ca_x)_3In_2Ge_3$ ($0.78 \leq x \leq 0.90$) Series[a]

	$(Eu_{1-x}Ca_x)_4In_3Ge_4$			$(Eu_{1-x}Ca_x)_3In_2Ge_3$	
atom pair	x = 0.70	x = 0.35	atom pair	x = 0.90	x = 0.78
M1−Ge1 (2×)	3.088(2)	3.123(1)	M1−Ge2 (2×)	3.080(2)	3.097(1)
M1−Ge2 (2×)	3.134(2)	3.173(1)	M1−Ge3 (2×)	3.123(2)	3.127(1)
M1−Ge2 (1×)	3.230(2)	3.269(1)	M1−Ge3 (1×)	3.223(3)	3.231(2)
M2−Ge1 (2×)	3.141(2)	3.172(1)	M2−Ge1 (2×)	3.137(2)	3.155(1)
M2−Ge1 (2×)	3.240(2)	3.283(1)	M2−Ge2 (2×)	3.212(2)	3.224(1)
M2−Ge2 (2×)	3.307(2)	3.347(1)	M2−Ge3 (2×)	3.312(2)	3.315(1)
			M3−Ge1 (2×)	3.072(2)	3.082(1)
			M3−Ge2 (2×)	3.115(2)	3.114(1)
			M3−Ge1 (2×)	3.152(2)	3.159(1)
In1−Ge1 (1×)	2.755(2)	2.776(1)	In1−Ge2 (1×)	2.760(2)	2.773(1)
In1−Ge2 (2×)	2.802(1)	2.819(1)	In1−Ge3 (2×)	2.790(1)	2.797(1)
In1−Ge2 (1×)	2.872(2)	2.887(1)	In1−Ge3 (1×)	2.861(2)	2.869(1)
In2−Ge1[b] (2×)	2.967(2)	2.986(1)	In2−Ge1[b] (1×)	2.895(2)	2.893(1)
In2−Ge2[c] (2×)	3.162(2)	3.211(1)	In2−Ge1[b] (1×)	2.898(2)	2.904(1)
			In2−Ge2[c] (1×)	2.935(2)	2.943(1)
			In2−Ge3[c] (1×)	3.288(2)	3.308(1)
Ge1−Ge1 (1×)	2.536(2)	2.541(2)	Ge1−Ge2 (1×)	2.533(2)	2.527(1)

[a] The refined distance for the intermediate compositions are given as Supporting Information. [b] Shorter bond. [c] Longer bond.

carbon tape. Their composition was analyzed on a JEOL 7400F electron microscope, equipped with an INCA-OXFORD energy-dispersive spectrometer. The microscope was operated at a 10 μA beam current at a 15 kV accelerating potential. The analysis was based on a total of six spots (50 μm in size, 120 s counting time) from two different needle-like crystals. The

established (averaged) ratio of the elements was Eu/Ca/In/Ge = 11.7:23.9:27.8:37.2. It is in good agreement with the composition $Eu_{1.23(1)}Ca_{2.77}In_3Ge_4$ (i.e., Eu/Ca/In/Ge = 11.2:25.1:27.3:36.4), obtained from the single-crystal refinement (Table 1).

Computational Details. Tight-binding, linear muffin-tin orbital (TB-LMTO) calculations[39] were carried out in the atomic sphere approximation (ASA) using the LMTO47 program.[40] Exchange and correlation were treated by the local density approximation.[41] All relativistic effects except spin−orbit coupling were taken into account by using a scalar relativistic approximation. In the ASA method, space is filled with overlapping Wigner−Seitz (WS) atomic spheres.[42] The symmetry of the potential is considered spherical inside each WS sphere, and a combined correction is used to take into account the overlapping part.[43] The radii of WS spheres were obtained by requiring that the overlapping potential be the best possible approximation to the full potential and were determined by an automatic procedure.[43] This overlap should not be too large because the error in kinetic energy introduced by the combined correction is proportional to the fourth power of the relative sphere overlap.[42] No empty spheres[42] were used. The WS radii are as follows: for the "4−3−4" series, Eu = 2.13 Å, Ca = 2.03 Å, In1 = 1.64 Å, In2 = 1.92 Å, Ge1 = 1.61 Å, and Ge2 = 1.47 Å, and for the "3−2−3" series, Ca and Eu = 2.06 Å, In1 = 1.62 Å, In2 = 1.85 Å, Ge1 = 1.58 Å, Ge2, and Ge3 = 1.45 Å. The basis sets included 6s, 6p, and 5d orbitals for Eu; 4s, 4p, and 3d orbitals for Ca; 5s, 5p, and 5d orbitals for In; and 4s, 4p, and 4d orbitals for Ge. The Eu 6p, Ca 3d, In 5d, and Ge 4d orbitals were treated by the Löwdin downfolding technique,[42] and the 4f electrons of Eu were treated as core electrons. In order to evaluate various orbital interactions, densities of state (DOS), the crystal orbital Hamilton populations (COHP) curves,[44] and the integrated COHP values (ICOHPs) were also calculated. The *k*-space integrations were conducted using the tetrahedron method,[45] and the self-consistent charge density was obtained using 236 and 130 irreducible *k* points in the Brillouin zone for the "4−3−4" series and the "3−2−3" series, respectively.

Results and Discussion

Structures and Phase Relationships. The quaternary $(Eu_{1-x}Ca_x)_4In_3Ge_4$ phase (Figure 1) crystallizes in the centrosymmetric space group $C2/m$, and its structure contains six crystallographically unique atoms in the asymmetric unit, all in special positions (Table 2). Formally, the structure can be classified with the monoclinic the Mg_5Si_6-type structure (Pearson's code *mS*22);[18] herein, M1 and M2 (both with mixed Eu and Ca) and In2 take the Mg sites, whereas Ge1, Ge2, and In1 atoms are placed at the Si sites of Mg_5Si_6. $(Eu_{1-x}Ca_x)_4In_3Ge_4$ is also isostructural to the quaternary germanide $RE_4Ni_2InGe_4$ (RE = Dy, Ho, Er, and Tm), reported recently by Salvador and Kanatzidis.[46] Unlike $RE_4Ni_2InGe_4$, which contains only one type of rare-earth metal as cations, the
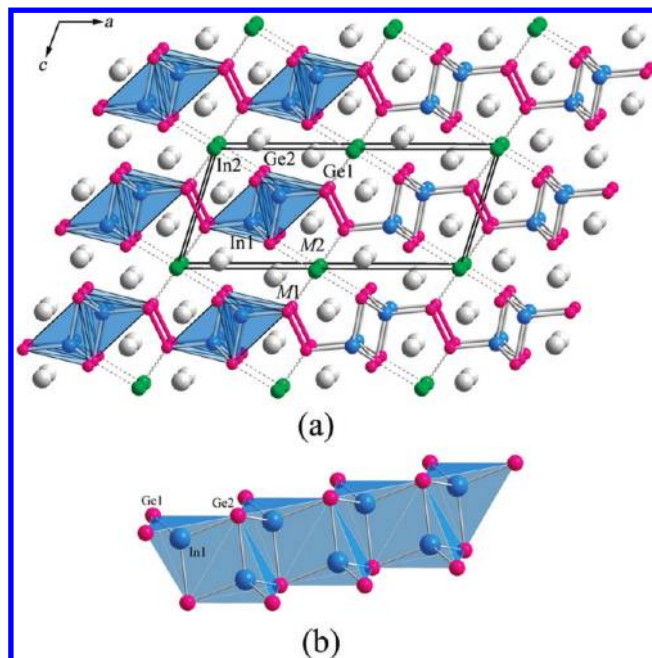

Figure 1. (a) Combined ball-and-stick and polyhedral representations of the crystal structure of the monoclinic $(Eu_{1-x}Ca_x)_4In_3Ge_4$ ("4−3−4" phase), viewed down the *b* axis. The layers made up of edge-shared $InGe_4$ tetrahedra, connected via Ge−Ge bonds, are highlighted. Color code: tetrahedral In (In1), blue; Ge, red; In2 (planar 4-coordinated) and the cations between the layers are shown in green and gray, respectively. (b) A closeup view emphasizing the connectivity of the $InGe_4$ tetrahedra.

"4−3−4" phase exists only with mixed cations (occupying the same sites). Another difference between the two structures is that the tetrahedral Ni position in $RE_4Ni_2InGe_4$ is occupied by an indium atom in $(Eu_{1-x}Ca_x)_4In_3Ge_4$; the other In position (In2 in the standardized settings) is "shared" between the two structures and will be discussed in greater detail later on.

The "4−3−4" structure (Figure 1a) can be readily described as polyanionic layers, $^2_\infty[InGe_2]$, running parallel to the *ab* plane and stacked along the *c* axis. They are made of one-dimensional chains of edge-shared $InGe_4$ tetrahedra (Figure 1b), propagating parallel to the crystallographic *b* axis. These chains are linked together via Ge_2 dimers in an orthogonal direction. Layers with similar topology, but made up of different elements, are also known for the isotypic $RE_4Ni_2InGe_4$[46] and the structurally similar $Ba_3Cd_2Sb_4$,[47] $Sm_3Co_2Ge_4$,[48] and $Ce_4Co_2Sn_5$.[49] The In−Ge ($d_{In-Ge} \approx 2.75-2.89$ Å) and Ge−Ge ($d_{Ge-Ge} \approx 2.54$ Å) distances within the polyanionic layers are slightly longer than the sum of the corresponding covalent radii ($r_{In} = 1.55$ Å; $r_{Ge} = 1.22$ Å),[50] in agreement with the predicted negative formal charges. These distances compare well with those reported for other compounds with two-center two-electron bonds: $d_{Ge-Ge} = 2.527-2.617$ Å in RE_3Ge_5 (RE = Sm, Gd, Tb, and Dy),[15] $d_{Ge-Ge} = 2.551$ Å in $EuGe_2$,[31] $d_{Ge-Ge} = 2.541$ Å

(39) (a) Andersen, O. K. *Phys. Rev. B* **1975**, *12*, 3060. (b) Andersen, O. K.; Jepsen, O. *Phys. Rev. Lett.* **1984**, *53*, 2571. (c) Andersen, O. K. *Phys. Rev. B* **1986**, *34*, 2439.
(40) Jepsen, O.; Burkhardt, A.; Andersen, O. K. *The TB-LMTO-ASA Program*, version 4.7; Max-Planck-Institut für Festkorperforschung: Stuttgart, Germany, 1999.
(41) Andersen, O. K.; Jepsen, O. *Phys. Rev. Lett.* **1984**, *53*, 2571.
(42) Andersen, O. K.; Jepsen, O.; Glötzel, D. In *Highlights of Condensed Matter Theory*; Bassani, F., Fumi, F., Tosi, M., Eds.; North-Holland: New York, 1985.
(43) Jepsen, O.; Anderson, O. K. *Z. Phys. B* **1995**, *97*, 35.
(44) Dronskowski, R.; Blöchl, P. *J. Phys. Chem.* **1993**, *97*, 8617.
(45) Blöchl, P. E.; Jepsen, O.; Anderson, O. K. *Phys. Rev. B* **1994**, *49*, 16223.
(46) Salvador, J. R.; Kanatzidis, M. G. *Inorg. Chem.* **2006**, *45*, 7091.

(47) Saparov, B.; Bobev, S. *Inorg. Chem.* **2008**, *47*, 11237.
(48) Mruz, O.; Fedyna, M. F.; Percharskii, V. K.; Bodak, O. I. *Izv. An. SSSR* **1989**, *12*, 2023.
(49) Pani, M.; Manfrinetti, P.; Palenzona, A.; Dhar, S. K.; Singh, S. *J. Alloys Compd.* **2000**, *299*, 39.
(50) Pauling, L. *The Nature of the Chemical Bond*; Cornell University Press: Ithaca, NY, 1960.
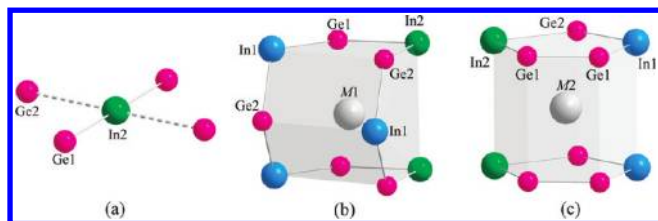
Figure 2. Magnified view of the local coordination of the In2 position (a). The cationic polyhedra of the M1 site (b) and the M2 site (c). Color code as in Figure 1.

in $CaGe_2$,[32] $d_{Ge-Ge} = 2.522$ Å and $d_{In-Ge} = 2.751$ Å in $EuInGe$,[33] $d_{Ge-Ge} = 2.575$ Å in Ca_5Ge_3,[51] $d_{In-Ge} = 2.806-2.904$ Å in $Ca_2LiInGe_2$ and $Sr_2LiInGe_2$,[52] and so forth. All In−Ge and Ge−Ge distances increase systematically as the compositions become Eu-richer.

Bridging In atoms in distorted square-planar coordination (In2, Figure 2a) and europium/calcium atoms are enclosed between the $^2_\infty[InGe_2]$ layers. The In2−Ge1 and In2−Ge2 distances fall in the range from 2.967(2) to 3.211(1) Å (Table 3)—noticeably longer than the aforementioned In1−Ge1 and In1−Ge2 contacts. They are also much longer than the sum of the covalent radii of In and Ge,[50] signifying weaker interactions. Similar in magnitude In−Ge distances are known for the RE_2InGe_2 (RE = La−Sm, Gd−Ho, Yb) phases,[5,17] where In is also 4-coordinated in the plane of its four nearest Ge atoms. Notice here that, in the tetragonal RE_2InGe_2 structure, all four In−Ge bonds are equivalent, while in the monoclinic $(Eu_{1-x}Ca_x)_4In_3Ge_4$, it may appear that In2 is connected to only two Ge atoms, as the opposing two Ge atoms are at distances which are about 8% longer (Figure 2a). The cations occupying the M1 site are surrounded by the five nearest Ge atoms, forming a distorted square-pyramid-shaped polyhedron (Figure 2b), with distances ranging from 3.088(2) to 3.267(2) Å. Five In atoms (capping edges) are located 3.554(2)−3.597(3) Å away. The coordination environment around the M1 site closely resembles the Yb environment observed in Yb_2CdSb_2.[23] The M2 site, in turn, is surrounded by six nearest Ge atoms (Ge1 × 4 and Ge2 × 2), with distances falling in the interval 3.141(2)−3.347(1) Å (Figure 2c). The four next-nearest In atoms are 3.383(4)−3.513(3) Å away, making the polyhedron appear somewhat as a ferrocene-like pentagonal prism. An almost identical coordination environment of Eu cations is known for $Eu_{11}Cd_6Sb_{12}$.[53]

Although Eu and Ca are not ordered, the refined occupations for different Eu/Ca ratios (Supporting Information) follow a trend, which is in agreement with the simple geometric reasoning—larger cations prefer the site with a higher coordination number, that is, M2. Further analysis of site preferences and the subtleties of the In−Ge bonding is carried out with the aid of the density-functional theory calculations and is discussed in the following section.

A better, and more rigorous from a crystallographic standpoint, description of the structure can be given once its close relationship with other ubiquitous structure

types is recognized—the CsCl, the AlB_2, and the TiNiSi.[18] Slabs bearing resemblance to the imaginary compounds $(Eu_{1-x}Ca_x)_2InGe_2$ with the Mo_2FeB_2-type structure (an intergrowth of the CsCl and the AlB_2 types)[18] and $(Eu_{1-x}Ca_x)_2In_2Ge_2$ with the TiNiSi-type structure can be immediately seen from the coloring scheme shown in Figure 3. Following this line of thought, the "4−3−4" structure can be conveniently rationalized as an intergrowth of these two structure types in a ratio of 1:1.[54] Accidentally, $(Eu_{1-x}Ca_x)_2InGe_2$ containing Eu, Ca, or mixed Eu/Ca atoms with the former structure was the sought-after phase in our designed experiments (vide infra), but it was never synthesized. Instead, this fragment "co-crystallizes" with the TiNiSi-like $(Eu_{1-x}Ca_x)_2In_2Ge_2$ slab, much as the imaginary YbGe and Yb_2MgGe_2 motifs coexist in Yb_4MgGe_4.[8] Using the same approach, it is evident that many other possible ways to combine such "2−1−2" and "2−2−2" fragments exist.[55] One of them is exemplified in the orthorhombic "3−2−3" structure, the next subject of our attention.

Assuming a homologous series $[A_2In_1Ge_2]_n[A_2In_2Ge_2]_m$, where A is a divalent cation (or mixed cations) and n and m are integers, one can readily see that $(Eu_{1-x}Ca_x)_4In_3Ge_4$ is the simplest member, described with $n = 1$ and $m = 1$. The next homologs should be realized when the two structures are combined in either a 2:1 or 1:2 ratio. Indeed, the $(Eu_{1-x}Ca_x)_3In_2Ge_3$ structure (or rather $(Eu_{1-x}Ca_x)_6In_4Ge_6$) is the member with $n = 2$ and $m = 1$, as depicted in Figure 3. This structure can also be described as the result of an insertion of an additional "2−1−2" slab into the structure of the "4−3−4" phase.

The quaternary $(Eu_{1-x}Ca_x)_3In_2Ge_3$ phase (Figure 4) crystallizes in the centrosymmetric space group $Pnma$, representing a new structure type with Pearson's code $oP32$. This structure contains eight crystallographically unique atoms in the asymmetric unit, all in special positions (Table 2). In and Ge form a polyanionic substructure, which is very similar to the one already discussed for the "4−3−4" phase—chains of edge-shared $InGe_4$ tetrahedra (In1, Ge2, and Ge3), running parallel to the crystallographic b axis. Each chain has two "handles", formed by linking together Ge1 and Ge2 atoms into dimers. These fragments are interconnected into a three-dimensional array via square-planar In (In2), with cations occupying the space within it (Figure 4). Eu and Ca are mixed on all three cation sites, even though the amount of Eu is generally small and the overall composition is close to that of the pure Ca analog. Therefore, all interatomic distances in this structure are slightly shorter than those found in $(Eu_{1-x}Ca_x)_4In_3Ge_4$ (Table 3). For example, the In1−Ge2 and In1−Ge3 distances are in the

(51) Mudring, A.-V; Corbett, J. D. *J. Am. Chem. Soc.* **2004**, *126*, 5277.
(52) Mao, J.-G.; Xu, Z.; Guloy, A. M. *Inorg. Chem.* **2001**, *40*, 4472.
(53) Saparov, B.; Bobev, S.; Ozbay, A.; Nowak, E. R. *J. Solid State Chem.* **2008**, *181*, 2690.
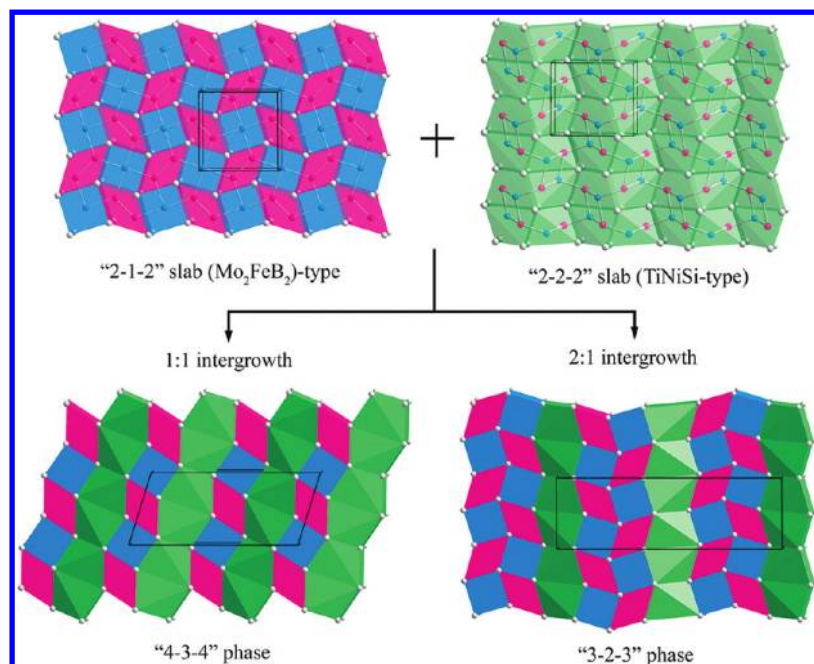
(54) A different way of describing this structure is through a structural transformation from a hypothetical $(Eu_{1-x}Ca_x)_4In_3Ge_4$ of the TiNiSi type, using the same imaginary cutting and pasting procedure, applied for the closely related $Ba_3Cd_2Sb_4$ structure (ref 47). This idea is depicted schematically in Figure S1 in the Supporting Information.
(55) Another parallel can be drawn with the recently reported $M_4Co_2Mg_3$ (M = Nd and Sm), which is a 1:3 intergrowth of MCo_2 and MMg slabs, with the AlB_2 and the CsCl structure types, respectively. In this case too, MCo_2 does not exist on its own and is stabilized by three MMg slabs. This structure resembles the "4−3−4" phase in terms of the arrangement of two structural segments—replacing two of the MMg's with a $MMgCo$ slab adopting the TiNiSi-type structure, we can also obtain the "4−3−4" phase.

Figure 3. Schematic illustration of the way the $(Eu_{1-x}Ca_x)_4In_3Ge_4$ ("4−3−4" phase) and $(Eu_{1-x}Ca_x)_3In_2Ge_3$ ("3−2−3" phase) can be assembled from slabs with the Mo_2FeB_2-type (alternating AlB_2 (red) and CsCl (blue)) and the TiNiSi-type (green) structures. See the text for a more detailed description.
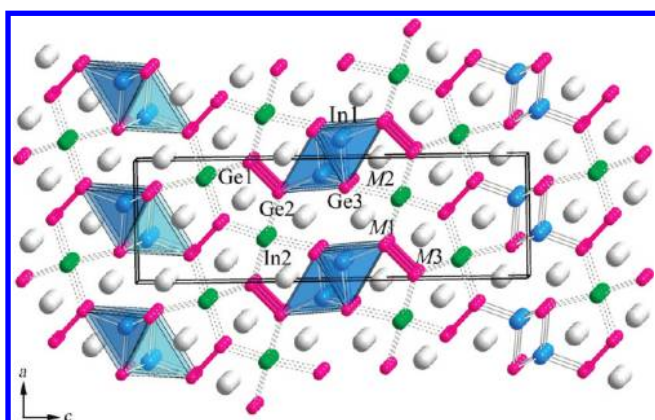

Figure 4. Combined ball-and-stick and polyhedral representations of the crystal structure of the orthorhombic $(Eu_{1-x}Ca_x)_3In_2Ge_3$ ("3−2−3" phase), viewed down the *b* axis. The $[InGe_2]$ chains of edge-shared $InGe_4$ tetrahedra, with the Ge_2 dumbbells as "handles" in the opposing ends, are emphasized. The square-planar In atoms interconnecting these fragments into a three-dimensional array and the Eu/Ca cations occupying the empty space are also shown. Color code: tetrahedral In (In1), blue; Ge, red; In2 (planar 4-coordinated) and the cations between the layers are shown in green and gray, respectively.

range 2.760(2)−2.869(1) Å, and the Ge1−Ge2 distances measure 2.527(1)−2.533(2) Å. However, one of the already weak bonding interactions of the planar In2 with its four Ge neighbors becomes even weaker, as can be inferred from the elongated distance ($d_{In2-Ge3} \approx 3.3$ Å).

Since the "4−3−4" and the "3−2−3" structures are topologically related, it is thus not surprising that the cations in both cases reside in similar Ge polyhedra with square-pyramidal (M1) and distorted-trigonal prismatic (M2, M3) geometries and have comparable distances (Table 3). The site preferences are also akin to each other, and despite the very low Eu content in some of the studied phases, none of the cationic sites is fully occupied by Ca atoms, but rather show at least 5% mixing with Eu.

We also point out that the M3 site has shorter M−M distances than the M1 and M2 sites, making it least likely choice for the larger Eu^{2+} cations.[21] This observation agrees very well with the theoretical considerations, discussed next.

Bonding and Electronic Structure. To examine the electronic structure and investigate the chemical bonding, calculations using the TB-LMTO-ASA method[40] were carried out. The calculations for the "4−3−4" phase were performed using an idealized "$Eu_2Ca_2In_3Ge_4$" structure, where Eu and Ca are ordered on the two cationic positions in the actual space group. For the "3−2−3" phase, the symmetry needed to be lowered from the actual space group *Pnma* to $P2_1/m$ in order to accommodate an idealized "$Eu_{0.5}Ca_{2.5}In_2Ge_3$" structure, where Eu and Ca are ordered on six independent positions. DOS and COHP curves for both structures are plotted in Figure 5.

As seen from Figure 5a, in the structure of "$Eu_2Ca_2In_3Ge_4$", there is significant valence orbital mixing among Eu, Ca, In, and Ge throughout the entire energy range. The occupied region of the DOS can be divided into four principal sections: (i) a region between −8.3 and −10.5 eV, which is dominated by Ge2 4s states with small contributions from In, Eu, and Ca; (ii) a region between −7.5 and −8.3 eV, which is mostly contributed by the other types of Ge 4s states with a small admixture of In, Eu, and Ca valence orbitals; (iii) a region between −4 and −6.5 eV, where the In 5s states are dominant; and (iv) a region between 0 and −4 eV, which includes a significant orbital mixing of Ge 4p and In 5p orbitals with Eu and Ca wave functions. The Fermi level (33 valence electrons) is located between two "local minima" of the total DOS (TDOS), within ca. ±0.35 eV from E_F corresponding to 32 and 34 valence electrons. According to the COHP analysis, the upper local minimum of TDOS matches the point where interatomic interactions,
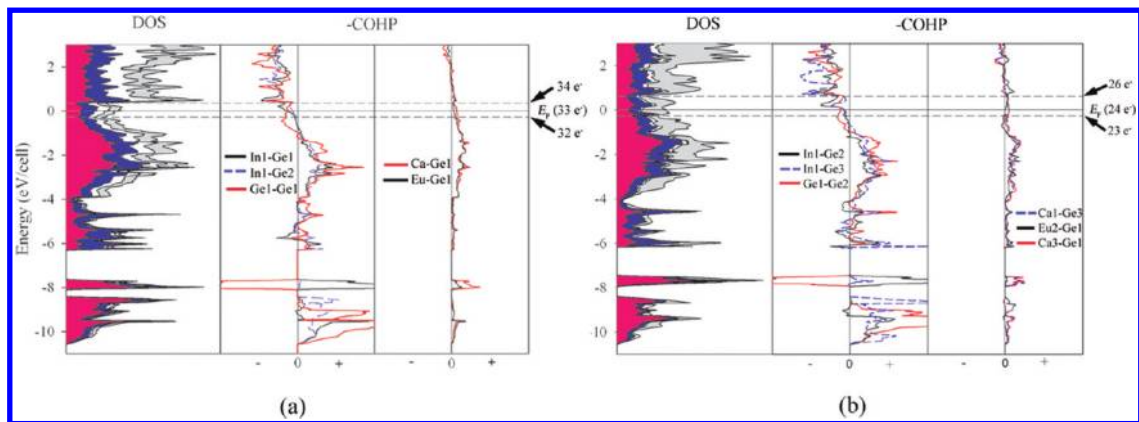
Figure 5. (a) DOS and COHP curves for the idealized "$Eu_2Ca_2In_3Ge_4$". (b) DOS and COHP curves for the idealized "$Eu_{0.5}Ca_{2.5}In_2Ge_3$". Total DOS is shown with a solid line; partial DOS of In is represented by the area shaded in blue, and the partial DOS of Ge is represented by the area in red. Eu and Ca PDOSs are represented by the white and gray regions, respectively. E_F (solid line) is the energy reference at 0 eV. Two adjacent local DOS minima and the corresponding numbers of valence electrons are also shown (dashed lines). In the −COHP curves, the "+" values are bonding interactions; "−" values are antibonding interactions, respectively.

such as In1−Ge1/Ge2 and Ge1−Ge1, begin to show significant antibonding character. Figure 5a (middle, right) displays In1−Ge1/Ge2, Ge1−Ge1, and Eu/Ca−Ge1 COHP curves. In1−Ge1 and In1−Ge2 COHP curves are nearly optimized at E_F, while Ge1−Ge1 shows considerable antibonding character. This is not surprising because this three-bonded (3b-Ge⁻) is in a trigonal-planar environment, instead of being in a preferred pyramidal, as observed in the corrugated $\frac{2}{\infty}[Ge_2]^{2-}$ layers in $EuGe_2$[31] and $CaGe_2$.[32] However, this antibonding character can be compensated by Ca−Ge1 and Eu−Ge1 interactions, which show bonding characters beyond +0.35 eV.

DOS and COHP curves for the "$Eu_{0.5}Ca_{2.5}In_2Ge_3$" structure are shown in Figure 5b. As can be expected from the similarity of the two structures, the characteristics of the bonding arrangements are alike. Thus, the DOS and COHP plots are qualitatively similar to those for "$Eu_2Ca_2In_3Ge_4$". The only noticeable difference, which of course is due to the smaller amount of Eu per formula unit, is the decreased overall Eu partial DOS (in particular the 5d band) and the less pronounced TDOS peak above the upper local DOS minimum at ca. +0.65 eV. The In1−Ge2/3 COHP curves corresponding to the indium in a tetrahedral coordination are nearly optimized at the Fermi level, and the Eu/Ca−Ge COHP curves show weak bonding interactions throughout the whole energy window.

As discussed earlier, in addition to the bonding within the polyanionic substructure, we were intrigued by the roles of the cations and studied the possible site preferences between Eu and Ca using Miller's approach dubbed "*the coloring problem*".[30] For this purpose, two hypothetical $Eu_2Ca_2In_3Ge_4$ structures with different occupations of the cation positions were derived: model **1**, in which Ca and Eu are ordered at the M1 and M2 site, respectively, and model **2**, with an alternative arrangement. The lattice parameters and atomic positions were taken from the crystallographic data for $Eu_{2.01(1)}Ca_{1.99}In_3Ge_4$, since its composition is closest to that of our model structures (see Table S2, Supporting Information). According to the total electronic energy comparison, model **1** is energetically favored over the alternative by 0.352 eV/f.u. Among the various contributions to the total energy, the band energy has the largest input to this structural preference.

Table 4. Results of the Tight-Binding Analysis of the Site-Energy and the Bond-Energy Terms in the Model Structures with Ordered Ca and Eu Cations[a]

	model **1**		model **2**
E_{TOT} (eV)	0.000		0.352
E_{Band} (eV)	0.000		0.351
Site Energies (eV)			
Ca (2×)	5.529		4.461
Eu (2×)	9.524		11.125
In1 (2×)	−3.889		−3.972
In2 (1×)	−6.182		−6.377
Ge1 (2×)	−42.109		−42.530
Ge2 (2×)	−45.947		−45.538
total	−83.074		−82.830
Bond Energies (eV)			
In1−Ge2[b] (2×)	−1.849		−1.842
In1−Ge2[c] (1×)	−0.770		−0.794
In1−Ge1 (1×)	−0.947		−0.943
In2−Ge2 (2×)	−0.751		−0.770
In2−Ge1 (2×)	−1.057		−1.058
Ge1−Ge1 (1×)	−1.204		−1.206
Ca2−Ge2 (2×)	−0.759	Eu2−Ge2 (2×)	−0.753
Ca2−Ge2 (1×)	−0.374	Eu2−Ge2 (1×)	−0.361
Ca2−Ge1 (2×)	−0.885	Eu2−Ge1 (2×)	−0.948
Eu2−Ge2 (2×)	−0.596	Ca2−Ge2 (2×)	−0.565
Eu2−Ge1 (2×)	−0.851	Ca2−Ge1 (2×)	−0.791
Eu2−Ge1 (2×)	−0.716	Ca2−Ge1 (2×)	−0.669
total	−10.756	total	−10.696
site + bond energies (eV)	−93.830		−93.526
relative total	0.000		0.304

[a] Model **1**: Ca at the M1 site and Eu at the M2 site. Model **2**: Eu at the M1 site and Ca at the M2 site. [b] Shorter bond. [c] Longer bond.

The band energy can be decomposed into a "site-energy" term and a "bond-energy" term: the "site-energy" term is calculated for each distinct site in the asymmetric unit by summing the products of occupation numbers and band centers for each atomic orbital, and the "bond-energy" term is evaluated by the ICOHPs. Adding all site-energy and bond-energy terms for the two structural models yields approximately the same difference as in the comparison of the calculated band energies. The small discrepancy arises because only the first nearest interatomic interactions are included in the bond-energy erm. The results of this analysis are summarized in Table 4.

Table 5. QVAL Values for Each Cation Site and Relative Total Energies in the Models Structures of "$Eu_{0.5}Ca_{2.5}In_2Ge_3$"[a]

	Eu at 50% of M1	Eu at 50% of M2	Eu at 50% of M3
	E/f.u. = +0.002 eV	E/f.u. = 0 eV	E/f.u. = +0.087 eV
M1	2.386	2.413	2.411
M2	2.507	2.472	2.506
M3	2.572	2.575	2.549

[a] The reported QVALs represent the averaged values between two cation sites in $P2_1/m$ (the symmetry of the model), which will be equivalent in $Pnma$ (the symmetry of the actual structure).

From the presented data, it is evident that model **1** is preferred with respect to both the site-energy and the bond-energy terms. Notice, in particular, the site energies of the ordered cations in **1** and **2**—they are, by far, the most lucid indicators, showing preference for the M2 site over the M1 site by 1.068 and 1.601 eV/f.u., for the Ca and Eu atoms, respectively. Summing all site energies yields 0.244 eV/f.u. lower energy for model **1** compared to model **2**, supporting the refinements of the site occupation factors in $Eu_{2.01(1)}Ca_{1.99}In_3Ge_4$ (Eu1/Ca1 = 30:70; Eu2/Ca2 = 70:30). In addition, the site preference is also confirmed by the bond-energy terms. A COHP analysis of the shortest Ca/Eu−Ge1/Ge2 interactions in **1** shows mostly larger ICOHP values than those in model **2**. Therefore, bond energies are also favored for model **1** by about 0.060 eV/f.u.

The site preferences among the three cationic sites in the "3−2−3" structure were also studied. For this purpose, three model structures were built as follows—a 50/50 mixture of Eu and Ca at either M1, M2, and M3 sites, with the remaining cationic sites fully occupied by Ca, giving rise to an idealized formula $EuCa_5In_4Ge_6$ (i.e., $Eu_{0.5}Ca_{2.5}In_2Ge_3$). The lattice parameters and atomic coordinates used in the calculations were obtained from the single-crystal refinement for $Eu_{0.52(1)}Ca_{2.48}In_2Ge_3$ (crystallographic information and schematic drawings can be found in the Supporting Information). In addition, the symmetry of the model structures was lowered to monoclinic with a space group $P2_1/m$ in order to describe the modified coloring of the cationic positions. The WS radii were kept constant. The total energy comparison indicates that the most energetically favorable one is the case where Eu substitutes Ca at the M2 site; substitutions at the M1 and M3 sites are uphill, by only ca. 0.002 eV/f.u. and 0.087 eV/f.u., respectively.

Since the total energy difference among the three models is rather small, and the distinction between the first two is somewhat unclear, we compared the quantity "QVAL" of each cation site.[56] Following this criterion, the more electronegative atom will be expected to occupy the site that has a higher density of valence electrons, that is, higher QVAL. Since the electronegativity of Eu is 1.01

(56) QVAL is calculated from the sum of the integrated electron densities within each WS sphere for atoms, and it approximates the valence electron number for each atomic site. It only *approximates* the number of valence electrons for each atomic site. Therefore, QVAL can *solely* be used for the comparison between different model structures or between different atomic sites, but not for determining the exact number of valence electrons in each orbital.
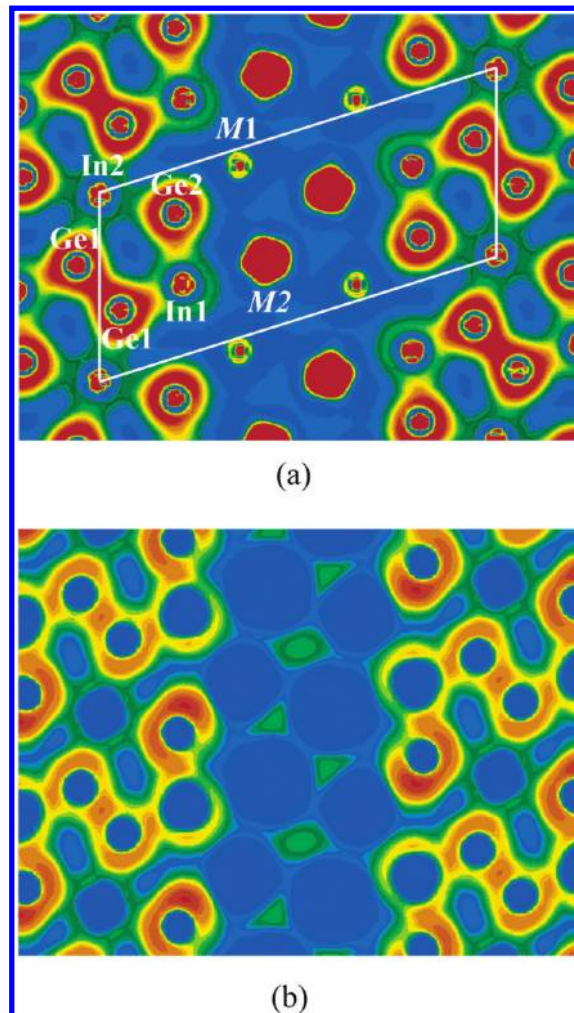
(57) WebElements Periodic Table of Elements. http://www.webelements.com (accessed Jan 2010).

Figure 6. Electron density map (a) and electron localization functions (ELF, b), calculated for the idealized "$Eu_2Ca_2In_3Ge_4$". Both plots are drawn for the (0 1 0) plane at zero height and are depicted as filled contour diagrams. The color scheme ranges from blue to orange (0.0−0.8) for ELF. Values of ELF exceeding 0.5 identify regions that exceed free-electron ELF values.

and the electronegativity of Ca is 1.04,[57] the M3 site, which has the largest QVAL in all cases (Table 5), should hence be least suitable for Eu. Such a conclusion is substantiated by the experimental results, where the lowest refined Eu occupation is always observed at the M3 site. It is also in good agreement with the trend inferred from the total energy calculations; however, theory and experiment are in a disagreement with regard to the M1 and M2 sites. Refinements indicate that Eu occupation is higher at the M2 site, while the calculations yield the lowest QVAL for the M1 site. This is suggestive of either a shortfall of the model or a need to do more sophisticated calculations with optimized structural parameters. After all, the "3−2−3" phase exists only for Ca-rich compositions and with a very small stoichiometry breadth (no conditions were found to extend it above 20 atom % Eu), which might indicate that there is very little energy profit from packing large and small cations in an ordered manner in this structure. The above could signify a delicate balance between the templating effect (governed by the ionic sizes) and the degree of covalency of the cation−anion bonding (expressed in the electronegativities)—the inability to
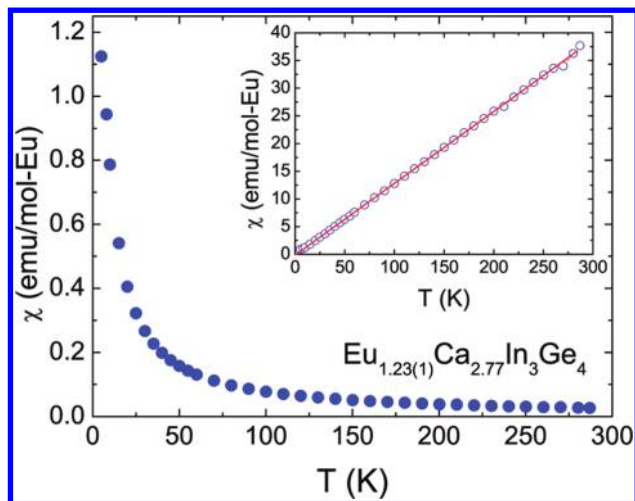
Figure 7. Temperature dependence of the magnetic susceptibility (χ_m) of $Eu_{1.23(1)}Ca_{2.77}In_3Ge_4$ single crystals, measured in a magnetic field of 500 Oe. The inverse magnetic susceptibility $\chi^{-1}(T)$ plot and a linear fit to the Curie–Weiss are shown in the inset.

synthesize either $Ca_3In_2Ge_3$ or the Sr analogs of $(Eu_{1-x}Ca_x)_3In_2Ge_3$ can be brought up as evidence for such conjecture (notice that the radii of Eu^{2+} ($r = 1.16$ Å) and Sr^{2+} ($r = 1.17$ Å) are nearly identical,[21] but the electronegativity of Sr is slightly lower than that of Eu, 0.99 versus 1.01, respectively).[57] This is in contrast with the simpler "4–3–4" structure, which shows definitive cation site preferences, but it is prone to a wide range of substitution patterns (vide supra). We can also speculate that, if there is such a trend in the formation of the "3–2–3" or any higher-order $[A_2In_1Ge_2]_n[A_2In_2Ge_2]_m$ homologs, for example "6–5–6" (for $n = 1$ and $m = 2$) or "8–5–8" (for $n = 3$ and $m = 1$), the latter will require a very different selection of cations. A testament to this line of thought is the partially refined structure of $(Ca_{1-x}Yb_x)_8In_5Ge_8$ (the predicted "8–5–8" phase, see the Supporting Information), which is realized only when the similar-sized but different in electronegativity Ca and Yb are used. Without more experimental data, it is difficult to make any predictions, although it seems likely that the electronic factors (i.e., the cation–anion mixing) take priority over the geometric factors (i.e., tendency for densest packing). Another such precedent, where there is a small size difference between the cations, and where the electronic factors are more influential to determining the site preference, was the recently reported $Gd_{5-x}Y_xTt_4$ (Tt = Si or Ge) series.

Last, we turn our attention to the planar In2 (Figure 2a), which deserves a special mention. Its unusual coordination and the very long In–Ge were discussed already, as well as the rhombic distortion, which leaves an open question—is this a linear or square-planar environment? In order to answer it conclusively, the electron density map and the electron localization function (ELF)[58] were analyzed. As shown in Figure 6, both plots are displayed in the *ac*-crystallographic plane

at $y = 0$. Looking at the ELF plot, the bond attractors in the midst of the Ge1–Ge1 dimer are clearly seen. They indicate the strong covalency of the interaction, as expected from the previously mentioned Ge–Ge distances. Lone pair-like electrons on the three-bonded Ge2 atoms should be noted too—they compose a pyramidal environment around the Ge atoms and are represented by large local ELF maxima.

The attractors around the In1–Ge1 bonds (within the tetrahedra) are also quite large and polarized around the Ge atoms. This, of course, is due to the difference in electronegativities between In and Ge. One can also observe sizable ELF values around the In2 atoms (between the layers), with attractors seen in all four directions, indicating that this In position should be considered as four-bonded. This analysis proves that weak but appreciable bonding In–Ge interactions exist in the plane, regardless of the long contacts (Table 3).

Magnetic Properties. Temperature-dependent dc magnetization measurements were performed for singe crystals of $Eu_{1.23(1)}Ca_{2.77}In_3Ge_4$. A plot of the magnetic susceptibility $\chi = M/H$ versus temperature T is shown in Figure 7. The temperature dependence is characteristic of a paramagnetic behavior due to localized f electrons. There are no indications of either short- or long-range magnetic order, and $\chi(T)$ follows the Curie–Weiss law $\chi(T) = N_A\mu_{eff}^2/3k_B(T - \theta_{CW})$[59] in the whole temperature interval (θ_{CW} is the Curie–Weiss constant). From the linear fit to the data (Figure 7, inset), an effective moment of $\mu_{eff} = 7.87$ μ_B per Eu^{2+} ion was calculated. Such a value agrees very well with the theoretically expected effective moment of 7.94 μ_B according to Hund's rules for the $[Xe]f^7$ configuration.[59] The corresponding θ_{CW} is on the order of +1 K, indicating very weak ferromagnetic coupling between the Eu^{2+} spins. No evidence for a magnetic phase transition is seen down to 5 K, although such could occur at lower temperatures (as can be inferred from the θ_{CW} value). All of the above confirms the stable divalent state of Eu in this structure. All attempts to probe the effect of the increased Eu content in $(Eu_{1-x}Ca_x)_4In_3Ge_4$ ($0.35(1) \le x \le 0.67(1)$) and $(Eu_{1-x}Ca_x)_3In_2Ge_3$ ($0.78(1) \le x \le 0.90(1)$) were unsuccessful due to the presence of secondary phases.

Conclusions

This article detailed the synthesis and structural characterization of the simplest members of a new homologous series of polar intermetallics, $A_{2[n+m]}In_{2n+m}Ge_{2[n+m]}$, where A stands for divalent alkaline-earth or rare-earth metals. The structures of $(Eu_{1-x}Ca_x)_4In_3Ge_4$ ($0.35(1) \le x \le 0.70(1)$) and $(Eu_{1-x}Ca_x)_3In_2Ge_3$ ($0.78(1) \le x \le 0.90(1)$) were established by single-crystal X-ray diffraction and can be best described as intergrowths of Mo_2FeB_2-like and TiNiSi-like fragments—a 1:1 intergrowth sequence for the former and 2:1 for the latter structure. Preliminary data suggest that the family can be extended and 3:1 intergrowths synthesized as well, provided the proper selection of the cations. All $A_{2[n+m]}In_{2n+m}Ge_{2[n+m]}$ phases exist only in mixed-cation systems and represent examples illustrating the strikingly delicate

(58) (a) Savin, A.; Flad, H. J.; Preuss, H.; von Schnering, H. G. *Angew. Chem.* **1992**, *104*, 185; Savin, A.; Flad, H. J.; Preuss, H.; von Schnering, H. G.; *Angew. Chem., Int. Ed. Engl.* **1992**, *31*, 185. (b) Kohout, M. *Int. J. Quantum Chem.* **2004**, *97*, 651. (c) Kohout, M.; Wagner, F. R.; Grin, Yu. *Theor. Chem. Acc.* **2002**, *108*, 150. (d) Gatti, C. *Z. Kristallogr.* **2005**, *220*, 399.

(59) (a) Smart, J. S. *Effective Theories of Magnetism*; Saunders: Philadelphia, PA, 1966. (b) Kittel, C. *Introduction to Solid State Physics*, 7th ed.; John Wiley and Sons: Hoboken, NJ, 1996.

balance between the atomic sizes and the orbital energies of the cations for the realization of a given crystal structure.

Since the Mo_2FeB_2- and TiNiSi-structure types are ubiquitous,[18] it could be expected that similar intergrowths will form with other elements. Further studies exploiting such reasoning are currently underway.

Supporting Information Available: A combined X-ray crystallographic file in CIF format, along with details of the synthesis, additional crystallographic information for the title compounds and for the recently synthesized higher-order homologue $(Ca_{1-x}Yb_x)_8In_5Ge_8$, a plot of the indexed powder diffraction pattern of $Eu_{1.23(1)}Ca_{2.77}In_3Ge_4$ (for which magnetization measurements were completed), plots of the crystal structures with anisotropic displacement parameters, and graphic representations of the model structures used in the computations. This material is available free of charge via the Internet at http://pubs.acs.org.